Cerebral Cortex, April 2021;31: 2139–2155

doi: 10.1093/cercor/bhaa351
Advance Access Publication Date: 7 December 2020
Original Article

ORIGINAL ARTICLE

Development of the Neuro-Immune-Vascular Plexus in the Ventricular Zone of the Prenatal Rat Neocortex

Elisa Penna[1,2], Jon M. Mangum[1,3], Hunter Shepherd[1,3], Veronica Martínez-Cerdeño[1,4,5] and Stephen C. Noctor[1,2]

[1]MIND Institute, School of Medicine, UC Davis, Sacramento, CA, USA, [2]Department of Psychiatry and Behavioral Sciences, School of Medicine, UC Davis, Sacramento, CA, USA, [3]Brigham Young University, Rexburg, Idaho, USA, [4]Department of Pathology and Laboratory Medicine, Institute for Pediatric Regenerative Medicine, School of Medicine, UC Davis, Sacramento, CA, USA and [5]Shriners Hospital, Sacramento, CA, USA

Address correspondence to Stephen C. Noctor, PhD, MIND Institute, School of Medicine, UC Davis, 2805 50th Street, Sacramento, California, 95817, USA. Email: scnoctor@ucdavis.edu.

Abstract

Microglial cells make extensive contacts with neural precursor cells (NPCs) and affiliate with vasculature in the developing cerebral cortex. But how vasculature contributes to cortical histogenesis is not yet fully understood. To better understand functional roles of developing vasculature in the embryonic rat cerebral cortex, we investigated the temporal and spatial relationships between vessels, microglia, and NPCs in the ventricular zone. Our results show that endothelial cells in developing cortical vessels extend numerous fine processes that directly contact mitotic NPCs and microglia; that these processes protrude from vessel walls and are distinct from tip cell processes; and that microglia, NPCs, and vessels are highly interconnected near the ventricle. These findings demonstrate the complex environment in which NPCs are embedded in cortical proliferative zones and suggest that developing vasculature represents a source of signaling with the potential to broadly influence cortical development. In summary, cortical histogenesis arises from the interplay among NPCs, microglia, and developing vasculature. Thus, factors that impinge on any single component have the potential to change the trajectory of cortical development and increase susceptibility for altered neurodevelopmental outcomes.

Key words: cortical development, microglial cells, neural precursor cells, proliferative zones, vascular development

Introduction

Microglial cells have emerged as active modulators in a growing number of developmental processes including synapse development and maintenance (Paolicelli et al. 2011; Schafer et al. 2012), axonal pathfinding (Squarzoni et al. 2014), and cortical layer formation (Ueno et al. 2013; Squarzoni et al. 2014). Microglia are present in the prenatal brain and we have shown that they are an intrinsic component of cortical germinal zones (Barger et al. 2019), establish extensive contacts with the neural precursor cells (NPCs) that generate cortical neurons and glial cells (Noctor et al. 2019), and regulate cortical cell production through phagocytosis of NPCs (Cunningham et al. 2013). The extensive contact and interactions between microglia and NPCs, neurons, and other glial cell types support the emerging concept that microglia are a key contributor to cortical development. As microglia begin colonizing the prenatal cortex, cortical vessels are established in the pial meninges, penetrate the underlying cortical parenchyma (Marin-Padilla and Knopman 2011), and are contacted by the processes of radial glial cells (Schmechel and Rakic 1979; Misson et al. 1988; Voigt 1989; Bentivoglio and Mazzarello 1999; Noctor et al. 2001). Determining whether and how development of the cortical vasculature coincides with or participates in cortical histogenesis requires a detailed map of vascular system development in relation to neurogenesis and microglial colonization. The goal of the current study is to establish a temporal map of vascular development in rat

cortical proliferative zones, in the context of neurogenesis and microglial colonization.

Neurogenesis begins in the rat neocortex by embryonic day (E)13 (Bayer and Altman 1991), and in human by the sixth week of gestation (Sidman and Rakic 1973). Microglia begin to colonize the rat and human cerebrum at the same stages of development (Andjelkovic et al. 1998; Verney et al. 2010; Cunningham et al. 2013). Development of cortical vasculature also follows a similar timeframe. A highly interconnected vascular structure termed the perineural vascular plexus, or pial capillary plexus, is present on the surface of the cerebrum by 6 weeks of gestation in human (Marin-Padilla and Knopman 2011; Engelhardt and Liebner 2014). The same structure is visible in rat by approximately E12 (Angelov and Vasilev 1989), and at the same stage of cortical development in other mammals (Marin-Padilla 1985; Bjornsson et al. 2015). We adopted the term 'pial vascular plexus' to highlight the location of this structure, and because these immature vascular structures will become arterioles, venules or capillaries at later stages of development (Marin-Padilla and Knopman 2011).

The pial vascular plexus is the source of vessels that supply the underlying cortical gray matter. Endothelial cells in the pial meninges pierce the external glial limiting membrane, extend filopodia and pseudopodia perpendicular to the pial surface that penetrate the basal lamina and extend toward the ventricle (Marin-Padilla and Knopman 2011; Mastorakos and McGavern 2019). Endothelial cells follow the path created by the filopodia, and form vessels that descend radially from the pial meninges toward the ventricle (Marin-Padilla 1985; Engelhardt and Liebner 2014; Bjornsson et al. 2015; Segarra et al. 2019). These radial vessels contribute to development of the first intrinsic capillary plexus to form in the developing cortex (Marin-Padilla and Knopman 2011), which we term the paraventricular plexus (PVP). The PVP courses within the ventricular zone (VZ) parallel to and near the ventricular surface.

Previous studies have noted individual relationships between cortical vessels, microglia and NPCs. Rezaie and Male highlighted a correlation between microglial position and cortical vessels in the developing cortex (Rezaie and Male 1999), proposing that these vessels serve as a route of microglial entry into the cortex. We previously examined the relationship between NPCs and periventricular microglia in the prenatal cortex and found extensive contacts between these two cell types (Cunningham et al. 2013; Barger et al. 2019; Noctor et al. 2019). Additionally, previous studies have shown that NPCs are often located near cortical vessels (Javaherian and Kriegstein 2009; Stubbs et al. 2009), and that endothelial cells influence NPC behavior (Shen et al. 2004). However, the relationships between NPCs, microglia, and cortical vasculature have not been studied together in the mammalian prenatal brain. The current study examines the concurrent development of these three systems, paying special attention to connectivity between these key elements.

Materials and Methods

Animals

All animal procedures were approved by the UC Davis Institutional Animal Care and Use Committee. Embryonic day (E)12 rat brains ($n = 4$), and E14 rat brains ($n = 4$) were fixed by direct immersion in 0.1 M phosphate-buffered saline pH 7.4 (PBS) containing (v/v) 4% paraformaldehyde (PFA) for 24 h. E16 ($n = 4$), E18 ($n = 4$), E19 ($n = 2$), E20 rat embryos ($n = 4$), and adult rats ($n = 2$) were transcardially perfused with PBS followed by 4% PFA. The brains were extracted and postfixed in 4% PFA for 24 h at 4°C. Care was taken to avoid damaging the meningeal layers covering the cerebrum. The next day brains were washed in PBS and stored in (v/v) 0.01% sodium azide in PBS at 4°C until processing for immunostaining. Cortical slabs were prepared from brains obtained from two E19 embryos by excising the dorsal portion of the cerebral cortex from each hemisphere using microscissors and an Olympus SZ61 dissecting scope (Noctor et al. 2019). The cortical slabs encompass the full thickness of the developing cerebral cortex spanning from the ventricle to the meningeal surface. The cortical slab approach was previously used and verified to maintain the physiological and morphological profile of radial glia cells (Noctor et al. 2002).

Immunohistochemistry

Brains were embedded into 4% Low Melt Agarose (Bio-Rad), sectioned 100 µm thick in the coronal plane on a Vibratome (Leica VT 1000), and free-floating sections collected in PBS. Sections were rinsed three times for 5 min each in PBS on a shaker and incubated in blocking buffer solution containing (v/v) 10% fetal donkey serum (Millipore); 0.1% Triton X-100 (Acros) in PBS for 2 h at room temperature (RT). Sections were then transferred to primary incubation buffer composed of (v/v) 2% fetal donkey serum, 0.02% Triton X-100 in PBS and primary antibodies: mouse monoclonal anti-vimentin (1:50, Millipore-Sigma Cat# V6630, clone V9, RRID: AB_477627); anti-phosphorylated vimentin (1:500, MBL: Cat# DO76-3S, clone 4A4, RRID: AB_592962); rabbit polyclonal anti-Iba1 (1:500 Fujifilm Wako Cat# 019-1974, RRID: AB_839504); rabbit monoclonal anti-PDGFR beta (1:500, Abcam Cat# ab32570, RRID: AB_777165); rabbit polyclonal anti-CD31 (1:500, Abcam Cat# ab28364 RRID: AB_726362), rabbit polyclonal anti-NG2 (1:500, Abcam Cat# ab129051); mouse monoclonal anti-alpha-smooth-muscle-actin (1:500, Abcam Cat# ab7817, RRID: AB_262054); and Isolectin GS-IB4 conjugated Alexa Fluor 568 (5 µg/mL, Invitrogen Cat# I21412, RRID: SCR_014365) overnight at RT. The next day sections were rinsed twice for 5 min in PBS, once for 5 min in (v/v) 0.1% Triton X-100 in PBS, and incubated for 2 h at RT in secondary antibody buffer containing (v/v) 2% fetal donkey serum, 0.02% Triton X-100, and donkey anti-mouse/anti-rabbit secondary antibodies conjugated respectively to Alexa Fluor 647 (1:500 Invitrogen Cat# A-31571, RRID: AB_162542) and Alexa Fluor 488 (1:500 Invitrogen Cat# A-32790, RRID: AB_2762833). Sections were rinsed three times for 5 min in PBS, stained with DAPI (Sigma-Aldrich, 1:1000) in PBS for 10 min, rinsed three times in PBS and cover-slipped with Mowiol 4-88 mounting medium (Sigma-Aldrich) and glass coverslips (Fisher).

Imaging

Sections and cortical slabs were imaged on an Olympus FV1000 IX81 confocal microscope with 40X water immersion (NA 0.7, Olympus) and 100X oil immersion (NA 1.3, Olympus) objectives. Sections obtained from the frontal, parietal–temporal, and occipital lobes were included in our analysis ($n = 4$ for each embryonic stage of gestation). Section thickness was constant (100 µm) and image stacks were acquired at 1.0 µm Z-steps using a 100X oil immersion objective. Sections were imaged at the ventricular surface and in the cortical gray matter and pial meninges. Image field of view was 130 mm^2; thus, images captured a maximum of 130 µm of tissue from the ventricular

surface through the proliferative zones, or pial surface through the gray matter, in the radial dimension. Z-stack series were only obtained from tissue sections that contained fully stained cells, contained the same number of Z-steps, and therefore saved images of labeled cells in the same volume of cortical tissue. Figures show projected images prepared from sequential confocal planes.

Fluoview Analysis

Images were analyzed using Olympus Fluoview software. In each Z-stack, we quantified the number of periventricular Iba1$^+$ somata and the number of principal processes, the number of processes that contacted blood vessels, the number of processes that contacted a 4A4$^+$ NPC soma, and/or 4A4$^+$ NPC pial process. We quantified the number of mitotic 4A4$^+$ NPCs that contacted Iba1$^+$ cells, and NPC soma or pial process that contacted blood vessels. We also quantified: the total number of IB4$^+$/Iba1$^-$ processes that sprouted from the surface of IB4-labeled blood vessels; the ratio of all IB4$^+$/Iba1$^-$ processes that extended toward to the ventricular surface versus the ratio of IB4$^+$/Iba1$^-$ processes that extended in all other directions from the vessel; the number of IB4$^+$/Iba1$^-$ processes that contacted the ventricular surface; and the number of IB4$^+$/Iba1$^-$ processes that contacted 4A4$^+$ NPCs and Iba1$^+$ cells. Contact was defined as two cell bodies/cell processes whose external surface(s) visibly touched each other or overlapped within a single Z-stack optical plane. Blood vessel diameter and distance between vessels were also quantified. Distance between blood vessels that arise from the pial vascular plexus and descend through the cortical plate was measured adjacent to the meningeal origin of the vessels. The distance between the ventricular surface and vessels in the PVP, the diameter of vascular loops in the PVP, and the distance between branch nodes in the PVP were measured across ages in the Z-stack optical planes.

Imaris Analysis

A 3D quantitative analysis of blood vessel volume and Iba1$^+$ cell volume within Z-stacks was performed using Imaris imaging software (Oxford Instruments America, Concord, MA). The total volumetric measure of reconstructed IB4$^+$ vessels and the volumetric measure of Iba1$^+$ structures was performed with Imaris software (shown in Fig. 5). The IB4$^+$ vessel volume was calculated as the percent IB4$^+$ volume occupied of the total volume within each Z-stack ($n = 3$ fields acquired from each cortical lobe at each embryonic age, $n = 3$ embryos per age). The Iba1$^+$ surface comprising cell soma and processes that overlapped with IB4$^+$ vessel structures was subtracted through channel segmentation and extracted from the image for analysis.

Statistics

Data are reported as mean ± standard deviation. Each data set was tested for normal distribution (D'Agostino-Pearson) and either parametric one-way ANOVA followed by Tukey's HSD post hoc test or non-parametric Kruskal–Wallis ANOVA followed by Dunn's post hoc test to statistically compare data sets across developmental stages using GraphPad Prism (GraphPad Software, Inc.). Test performed and P values are reported in figure legends. $P < 0.05$ was considered significant.

Results

Microglial cells do not distribute evenly across the cortical wall after entering the prenatal brain—as seen in the mature cerebral cortex—but populate specific laminae including the cortical germinal zones. Furthermore, microglia do not distribute uniformly within the proliferative zones but occupy specific positions in the proliferative zones in a pattern that we have observed in multiple vertebrate species (Cunningham et al. 2013; Noctor et al. 2019). A distinct single cell layer of microglia becomes apparent near the boundary of the VZ and subventricular zone (SVZ) during mid to late stages of cortical neurogenesis (arrowheads, Fig. 1). We term these cells periventricular microglia (Noctor et al. 2019). Periventricular microglia are highly integrated in the VZ and make extensive contacts with mitotic NPCs (Barger et al. 2019; Noctor et al. 2019). To better understand the function of periventricular microglia, we examined their distribution and morphology in the context of cortical vasculature. We labeled cortical vessels with the glycoprotein marker isolectin B4 (IB4), microglia with antibodies against the calcium-binding protein Iba1, mitotic NPCs with antibodies against phosphorylated vimentin (4A4), interphase NPCs with anti-vimentin antibodies, and cell nuclei with DAPI. We also tested for the presence of cell types that compose cortical vessels: endothelial cells with anti-CD31 antibodies, smooth muscle cells with antibodies against vascular smooth muscle α-actin (α-SMA), pericytes with antibodies against platelet-derived growth factor receptor β (PDGFR-β), and astroglia with anti-vimentin antibodies. Coronal sections or cortical slab preparations obtained from the neocortex of embryonic and adult rats were labeled with sets of four markers and imaged on a confocal microscope.

Basic Vascular Development During Corticogenesis

We investigated the appearance and formation of vessels in the neocortex in the context of neurogenesis at five stages of prenatal rat development between E12—the onset of cortical neurogenesis in rat, and E20—near the end of cortical neurogenesis for layer 2 neurons in rat (Bayer and Altman 1991).

E12: The E12 rat occipital cortex is thin, measuring approximately 140 µm from ventricle to the superior surface of the pial meninges. The pial vascular plexus becomes apparent first as a collection of IB4$^+$ cells arranged linearly within the meningeal layer of the forebrain (red cell indicated with white arrow, Fig. 2A). Thin descending IB4$^+$ vessels that appeared patent were visible (white arrowheads, Fig. 2A), and often connected with IB4$^+$ vessels oriented parallel to the ventricle (yellow/black arrowheads). The descending vessels were very thin, often appearing as individual cells or undifferentiated capillaries (Engelhardt and Liebner 2014), and measured 5.6 ± 1.6 µm in diameter. A growing collection of vessels that ran parallel to the ventricle within the VZ (yellow/black arrowheads, Fig. 2A) were 5–10 µm wide and marked the development of the intrinsic cortical plexus that we term the PVP. A small number of Iba1$^+$ microglia were present in the E12 cortex as we previously reported (Cunningham et al. 2013). Most Iba1$^+$ cells (green) also stained positive for IB4 (red) at this stage of development and appeared yellow (yellow asterisk, Fig. 2A). The proliferative zone comprised 4A4$^+$ NPCs undergoing division at the margin of the ventricle, and sparse 4A4$^+$ cells dividing away from the ventricle (white cells, Fig. 2A).

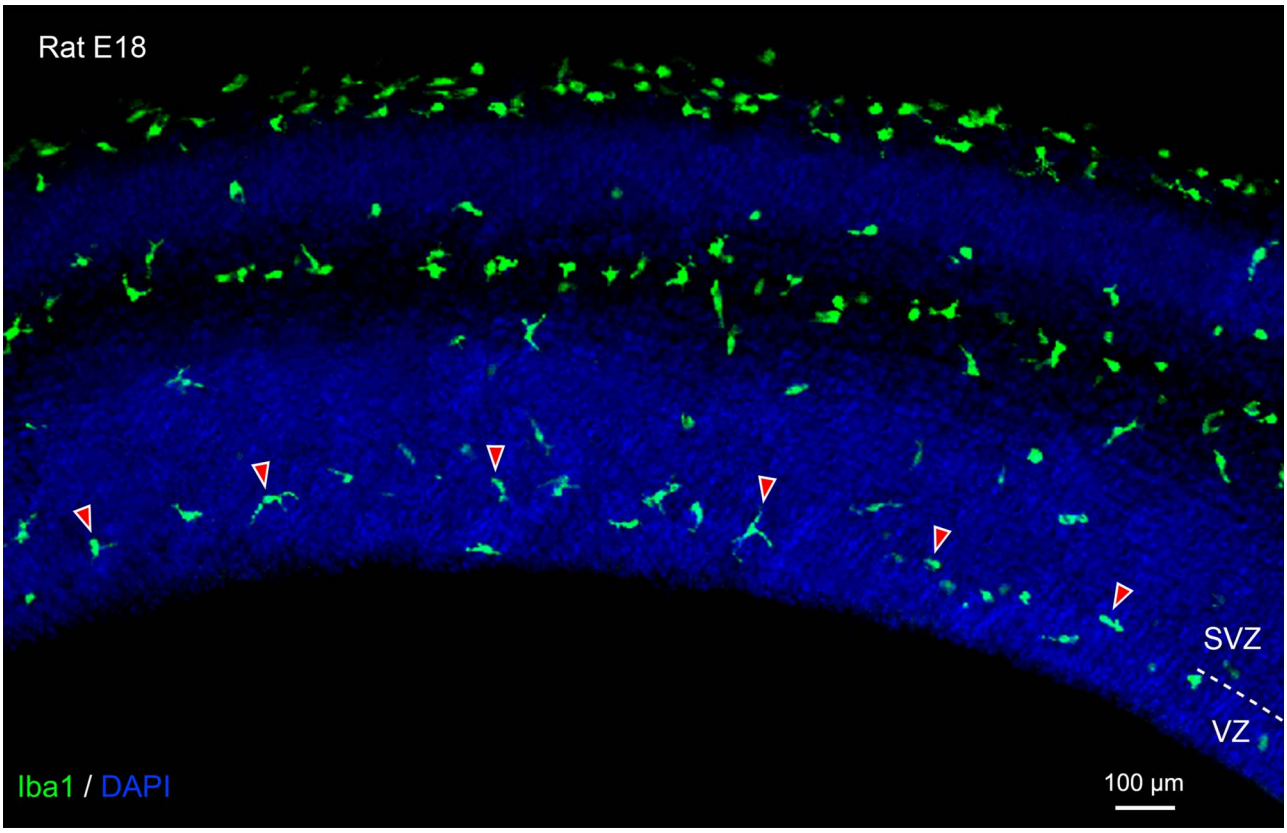

Figure 1. Periventricular microglial cells (green, Iba1) initially localize to the boundary between the ventricular zone (VZ) and subventricular zone (SVZ). In this image from an embryonic day (E)18 rat, arrowheads highlight a few of the periventricular microglia. Demarcation between the VZ and SVZ indicated by dashed line on right side of image. Blue, DAPI.

E14: The E14 occipital cortex remained thin at 165 μm, but the pial vascular plexus was appreciably thicker and more developed at this age. Well-formed ~10 μm-wide vessels descended from the pial vascular plexus toward the ventricle and connected with vessels in the PVP coursing parallel to the surface of the ventricle (yellow/black arrowheads, Fig. 2B). Vessels in the PVP were 9.6 ± 3.6 μm in diameter and coursed longer distances parallel to the lumen surface (yellow/black arrowheads, Fig. 2B). There was a small increase in the number of Iba1$^+$ microglial cells (green), most of which were also IB4 positive (yellow). The proliferative zone consisted of 4A4$^+$ NPCs undergoing division at the surface of the lumen, and a slightly increased number of 4A4$^+$ cells dividing away from the ventricle (white cells, Fig. 2B), as we previously reported (Noctor et al. 2008).

E16: The E16 rat cortex was significantly thicker at 315 μm. The thickness of the pial vascular plexus at E16 remained similar to that at E14. However, an increased number of cortical vessels descended from the pial vascular plexus through the developing gray matter (Fig. 2C). The descending vessels were located at regular intervals, with an average distance of 84 ± 23.02 μm between vessels (Fig. 2G). There was also an increased complexity in the pattern of cortical vessel branching. Vessels penetrated the developing gray matter, branched, and gave rise to collateral branches that formed an intrinsic cortical plexus within deeper cortical layers and white matter, as previously reported (Marin–Padilla 1995; Marin-Padilla and Knopman 2011). From the intrinsic cortical plexus emerged a complex pattern of vessels that descended both radially and at a 45° angle, ultimately reaching the PVP near the ventricle. Despite the increased thickness of the cortical wall and proliferative zones, vessels in the PVP remained at a constant 30 μm from the ventricle (yellow/black arrowheads, Fig. 2F). There was a slight increase in the number of Iba1$^+$ microglial cells at E16 (green). While most cortical microglia were IB4-positive, an increasing number of microglia in the meningeal layer were IB4-negative (Fig. 2C). Mitotically active 4A4$^+$ cells divided at the surface of the ventricle, and in the nascent SVZ (white cells, Fig. 2C).

E18: The E18 rat cortex was 490 μm thick. The pial vascular plexus remained similar to that at E14 and E16 (Fig. 2D). There was a further increase in the number of cortical vessels that descended from the pial vascular plexus through the developing gray matter at an average distance of 62.8 ± 19.7 μm from one another (Fig. 2G). There was a further increase in the complexity of cortical vessel branching, with an intrinsic cortical plexus apparent under the cortical plate and in the SVZ, in addition to the PVP near the ventricle. There were more Iba1$^+$ microglial cells at E18 (green). A few of the microglia also stained strongly positive for IB4, but the majority of microglia stained very lightly or were negative for IB4 (Fig. 2D). Mitotically active 4A4$^+$ cells divided at the surface of the ventricle and in the well-established SVZ (white cells, Fig. 2D).

E20: The E20 rat cortex measured 580 μm thick and exhibited complex vascular patterns and microglial cell distribution. A greater number of cortical vessels descended from the pial vascular plexus through the cortical plate at regular intervals of 48 ± 4.2 μm in the coronal sections (Fig. 2E), which was

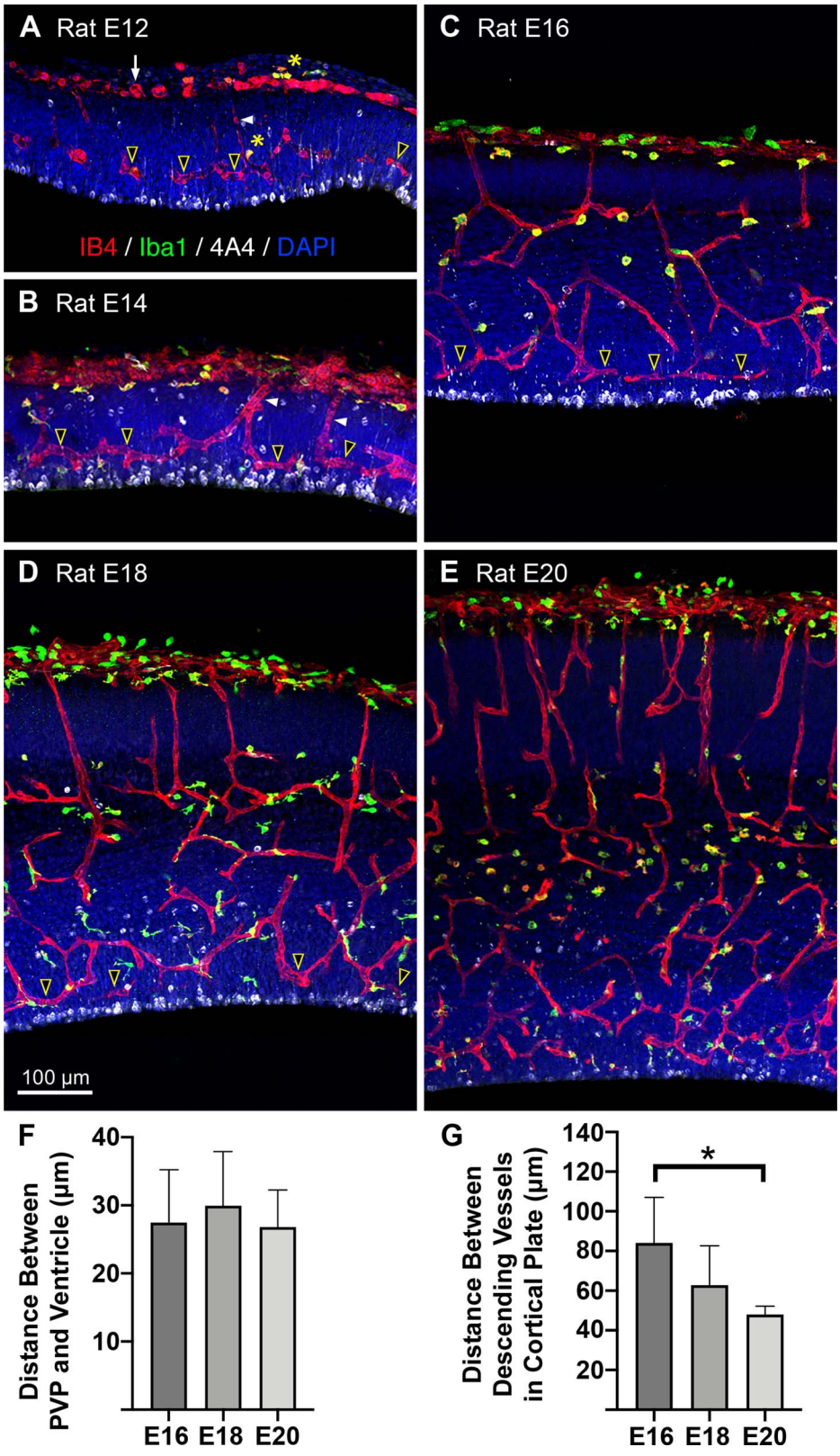

Figure 2. Basics of vascular development during cortical neurogenesis. Panels show the location of vessels (red, IB4), microglia (green, Iba1), and mitotic NPCs (white, 4A4) in coronal sections from the occipital lobe of embryonic rats (E) between E12 to E20. DAPI stained cells, blue. (A) The pial vascular plexus becomes apparent as a collection of $IB4^{+}$ cells and vessels within the pial mater (white arrow). Very thin $IB4^{+}$ vessels descend from the pial vascular plexus (white arrowhead) toward the ventricle. A growing collection of vessels that run parallel to the ventricle, within the VZ (yellow/black arrowheads), and approximately 30 µm from the ventricle marked the development of the paraventricular plexus (PVP). Mitotic NPCs (white, 4A4) line the ventricle and a few dividing cells are visible away from the ventricle. *(legend continued on next page)*

significantly closer than vessels in the E16 brains (Kruskal–Wallis ANOVA, Dunn's test, $P < 0.01$, Fig. 2G). The number of intrinsic cortical plexuses increased as previously described (Marin-Padilla 1995), and were apparent under the cortical plate, in the white matter, throughout the proliferative zones, and at the surface of the ventricle. The expansion of the PVP into the SVZ became apparent. The number of Iba1$^+$ microglial cells also increased, with some microglia exhibiting various morphological profiles staining intensely positive for IB4, while other microglia were lightly stained or IB4-negative (Fig. 2E). Mitotically active 4A4$^+$ cells divided at the edge of the ventricle and in the SVZ (white cells, Fig. 2E).

The PVP is a Dense Bed of Anastomotic Loops Adjacent to the Ventricle

The PVP is the first intrinsic cortical plexus to be established in the prenatal forebrain (Marin-Padilla and Knopman 2011), and is apparent in the VZ soon after the pial vascular plexus forms in the meninges. Because the PVP forms near the margin of the ventricle where NPCs divide, because it forms at the onset of cortical neurogenesis, and because there are abundant contacts between periventricular microglia and mitotic NPCs in this location (Barger et al. 2019; Noctor et al. 2019), we more closely examined vessels in the PVP.

To visualize the organization of vessels in the PVP, we imaged IB4$^+$ vessels near the ventricle *en face* in cortical slabs preparations dissected from E19 rats (Noctor et al. 2019). This plexus consists of vessels arranged in a repeating pattern formed by the adjoining branches of vessels anastomosing in circular loops near the ventricle. The anastomotic loops measured 70.0 ± 9.1 µm in diameter ($n = 68$, see Fig. 3), many of which appeared pentagonal or hexagonal in shape, and had 5 or 6 branches that joined neighboring anastomotic loops. Across development, the PVP remained approximately 30 µm from the ventricular surface (Fig. 2F). Thus, the PVP is a dense vascular bed comprising a continuous sheet of interconnected loops situated just superficial to mitotic NPCs, and that extends along the entire lateral ventricle in dorsal cortex of embryonic rat brains.

We next examined vessels in the PVP at higher magnification in coronal sections prepared from E12—E20 embryos. Imaging of the PVP vessels was performed with a 100X objective on cortical tissue adjacent to the lateral ventricle and producing a field of view that included up to 130 µm of tissue in the radial dimension and 130 µm in the tangential dimension. Many vessels in the PVP ran parallel to the ventricle, as seen en face in Fig. 3, but vessels that coursed perpendicular to the ventricle, for example connecting with the pial vascular plexus, and in other orientations were also observed. All vessels in the PVP were highly branched and anastomotic, and thus the average length of vessel segments between branching or anastomotic nodes was just 45 µm (E16: 44.4 ± 12.6 µm; E18: 41.4 ± 13.9 µm; E20: 45.3 ± 14.8 µm).

Microglia are Highly Integrated with PVP Vessels

We examined vessels of the PVP in tissue counterstained with the Iba1 antibody and found that, with few exceptions, periventricular microglia directly contacted vessels. The vast majority of microglial cells were located adjacent to, on, or tightly integrated within IB4$^+$ vessels (Fig. 4). We observed microglial cell bodies in direct contact with vasculature, in some cases showing somata wrapped around cortical vessels. Some of the microglia appeared to migrate along vessels, and other microglia were otherwise attached to vessels, appearing to 'embrace' vasculature with two or three processes. Finally, some microglia were positioned close to vessels, at a distance of one or two cell bodies, but extended cellular processes that contacted vasculature (Fig. 4C). We quantified the proportion of microglia contacting vessels in the VZ, and it remained above 80% throughout the neurogenic period. At E14, 82.2 ± 16.8% of microglia-contacted blood vessels; at E16, 86.3 ± 17.5% of microglia were in contact with cortical vessels; at E18, 84.9 ± 7.3% of microglia contacted vessels; and at E20, 90.1 ± 8.7% of microglia contacted vessels (Fig. 4E). These findings matched previous descriptions of microglial cells that noted their location adjacent to and within cortical vessels (Rezaie and Male 1999).

Numerous Filopodia Extend from PVP Vessels

Numerous fine processes extended from IB4$^+$ vessels in the PVP. Previous work has described cortical vasculogenesis, in particular that the growing ends of new vessels are often marked by tip cells that extend filopodia (Marin-Padilla and Knopman 2011). In addition to tip cells, we noted numerous filopodia that extended from vessel walls, particularly near the ventricle (Fig. 5). The diameter of these thin processes ranged from less than 0.1 to

Figure 2 continued: Very few microglial cells were present in the cortex at E12 (green, Iba1), and also stained positive for IB4$^+$ (red) and thus appeared yellow (yellow asterisks). (*B*) At E14 the pial vascular plexus was thicker and more developed. Well-formed capillaries descended toward the ventricle and connected with vessels in the PVP that coursed parallel to the ventricle (yellow/black arrowheads). There was a small increase in the number of Iba1$^+$ microglial cells (green), which also were mostly IB4$^+$ (yellow). 4A4$^+$ NPCs dividing at the surface of the lumen away from the ventricle are visible (white). (*C*) E16, the pial vascular plexus was similar to E14, but an increased number of vessels descended through the cortical plate. Descending vessels were located at regular intervals approximately every 85 µm. Increased branching gave rise to collateral branches forming an intrinsic cortical plexus within deeper cortical layers and the white matter. Vessels descended from the intrinsic cortical plexus to connect with the PVP, which remained about 30 µm from the ventricle (yellow/black arrowheads). Slightly increased Iba1$^+$ microglia (green) were apparent. Most microglia stained positive for IB4, but an increasing number were IB4 negative. Mitotically active NPCs (white, 4A4) divided at the ventricle and in the SVZ. (*D*) E18, we noted an increased number of descending vessels located more closely together (~63 µm), and increased complexity of vessel branching below the cortical plate and in the SVZ. The PVP near the ventricle was thicker in the radial dimension (yellow/black arrowheads). A larger portion of cortical microglia stained very lightly or negative for IB4. Dividing NPCs were visible at the surface and in the well-established SVZ (white). (*E*) E20, a greater number of vessels descended through the cortical plate at closer intervals than at earlier stages (48 µm). Intrinsic cortical plexus' increased in number and complexity under the cortical plate, in the white matter, throughout the proliferative zones. The PVP comprised was thicker, comprising vascular loops at multiple levels. Increased Iba1$^+$ microglia (green) with various morphological profiles staining intensely positive for IB4, while other microglia were lightly stained or IB4-negative. Mitotically active 4A4$^+$ cells divided at the ventricle and in the SVZ (white cells). (*F*) Histogram showing that the PVP remained approximately 30 µm from the ventricle across development. This position placed vessels directly superficial to actively dividing NPCs during principle stages of cell genesis. One-way ANOVA showed no significant differences between groups. (*G*) Histogram showing that the distance between vessels descending from the pial vascular plexus through the cortical plate decreased across development. Inter-vessel distance was significantly decreased at E20 compared to E16 (Kruskal–Wallis ANOVA, Dunn's post hoc test, $^*P < 0.01$). The decreased distance between vessels correlated with an increased number of vessels serving cortical tissue as the size of the cortex expanded. Scale bar in *D* applies to panels *A*-*E*.

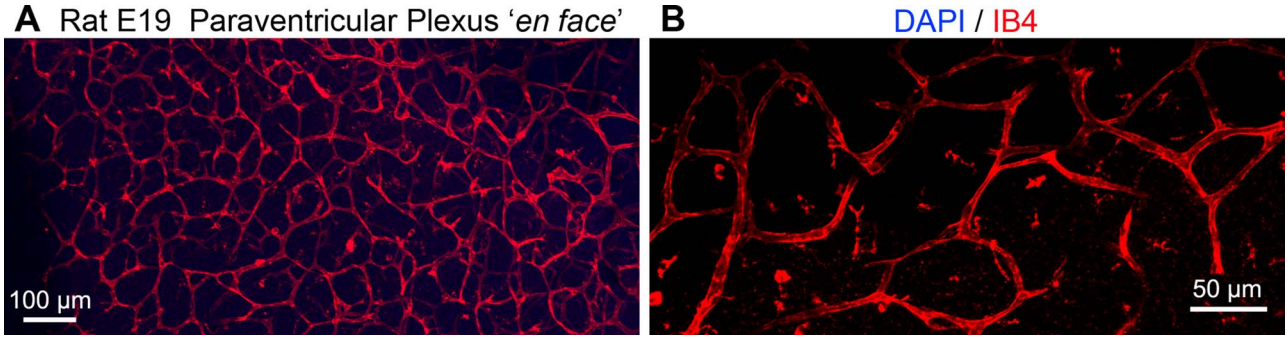

Figure 3. En face image of the lateral ventricle surface in embryonic day (E)19 rat cerebral cortex. (*A*) Low power images show the repeating pattern of vessels arranged in a repeating pattern formed by the adjoining branches of vessels anastomosing in circular loops near the ventricle. The anastomotic loops measured about 70 µm in diameter. (*B*) Higher power image showing the dense bed of anastomotic loops in the paraventricular plexus adjacent to the ventricle.

0.5 µm in diameter and varied in length from 2 to 40 µm in the PVP. Microglia were closely affiliated with blood vessels and also extended processes into the surrounding parenchyma. In order to differentiate vascular filopodia from microglial processes, we co-stained all sections with the microglial marker Iba1 and subtracted Iba1$^+$ microglial processes from our analysis of filopodia (red/white dots in Fig. 5*A–C*). We quantified the length and the number of processes extending from PVP vessels at E16, E18, and E20 (Fig. 5*E*). At E16, the average length of filopodia extending from PVP vessels was 9.7 ± 7.8 µm; at E18, filopodia averaged 12.7 ± 13.3 µm in length; and at E20, averaged 9.0 ± 7.9 µm in length. There was a large degree of variability in process length, and greater than 65% of filopodia were longer than 5 µm at each age.

A greater number of filopodia extended from vessels in the PVP close to the ventricle compared to descending vessels and vessels at other levels in the cortical wall. We compared the number of filopodia extending from vessels in the PVP versus those extending from vessels in the pial vascular plexus at two stages of development. We quantified filopodia number in the PVP and pial vascular plexus at E16 before the SVZ forms, and at E18 after formation of the SVZ during peak cortical neurogenesis in the rat (Bayer and Altman 1991). At E16, vessels in the PVP extended 32.1 ± 14.3 filopodia per field, while vessels in the pial vascular plexus extended just 5.2 ± 3.3 filopodia per field of view. At E18, vessels in the PVP extended 18.3 ± 6.9 filopodia versus 2.1 ± 1.8 filopodia from vessels in the pial vascular plexus.

Filopodia Extend toward the Ventricle and Contact Mitotic Precursor Cells

We observed that while filopodia processes extended from the IB4$^+$ vessels in all directions, the majority was oriented toward the ventricular surface (Fig. 6). At E14, $80.1 \pm 2.6\%$ of PVP filopodia extended toward the ventricle; at E16, $61.5 \pm 11.8\%$ extended toward the ventricle; at E18, $62.2 \pm 11.0\%$; and at E20, $63.5 \pm 6.4\%$ of PVP filopodia extended toward the ventricle. At each age, significantly more filopodia were directed toward the ventricle compared to all other directions (ANOVA, Tukey's post hoc, $P < 0.01$ Fig. 6*J*). The length of the longer filopodia defined the distance between vessels in the PVP and the surface of the ventricle, where radial glia undergo mitosis.

Filopodia that reached the ventricle were often marked by varicosities along the process and bouton-like swellings at the terminal end (Fig. 6). Furthermore, filopodia varicosities and terminal endings aligned with connexin-43 (Cx43) immunoreactivity (Figs 6*B–D*), indicating the potential for intercellular communication via gap junctions or hemi-channels between filopodia and NPCs at the surface of the ventricle. The pattern of Cx43 expression we observed in the embryonic rat is consistent with previous work in the embryonic mouse (Cina et al. 2007; Elias et al. 2007).

Co-staining with IB4 and 4A4 showed that vascular filopodia contacted mitotic NPCs (Fig. 6*E*). Analysis of high-magnification images in confocal Z-stacks showed that some filopodia terminated within the sphere of 4A4$^+$ dividing NPCs (Figs 6*F–I*). We previously observed that microglial cell processes also terminate within the sphere of 4A4$^+$ NPCs (Noctor et al. 2019). Our images indicate that mitotic NPCs have a complex outer membrane that includes grooves or channels through which vascular filopodia course, and support the concept of direct intercellular communication between endothelial cells and NPCs.

We quantified the proportion of filopodia that reached the ventricle and/or contacted mitotic NPCs. At E16, $25.1 \pm 14.2\%$ of ventricle-oriented filopodia reached the surface of the ventricle, and $13.5 \pm 10.1\%$ of the filopodia terminated on 4A4$^+$ mitotic NPCs. At E18, $17.9 \pm 12.1\%$ reached the ventricular surface and $23.2 \pm 18.6\%$ terminated on 4A4$^+$ mitotic NPCs. At E20, the percentage of PVP filopodia that reached the surface of the ventricle fell to $6.3 \pm 9.7\%$, and the percentage that contacted 4A4$^+$ mitotic NPCs was just $2.3 \pm 4.2\%$. The lower number of filopodia contacting NPCs at E20 corresponds with the reduction in mitotic divisions at the surface of the ventricle in embryonic rats at the end of cortical neurogenesis (Martinez-Cerdeño et al. 2012). The high standard deviation resulted from vessel segments in the PVP that had a few short filopodia that did not reach the ventricle or visibly contact mitotic NPCs.

Filopodia Extend from Endothelial Cells

The majority of filopodia extended from IB4-labeled vessels. Since blood vessels are composed of multiple cell types, and since microglia were tightly integrated with blood vessels in the embryonic cortex, we investigated the composition of the IB4$^+$ vessels in the PVP to identify the source of the filopodia. Mature blood vessel walls are composed of endothelial cells, smooth muscle cells, pericytes, and processes from astroglial cells (Engelhardt and Liebner 2014; Iadecola 2017; Kisler et al. 2017; Mastorakos and McGavern 2019). We stained embryonic

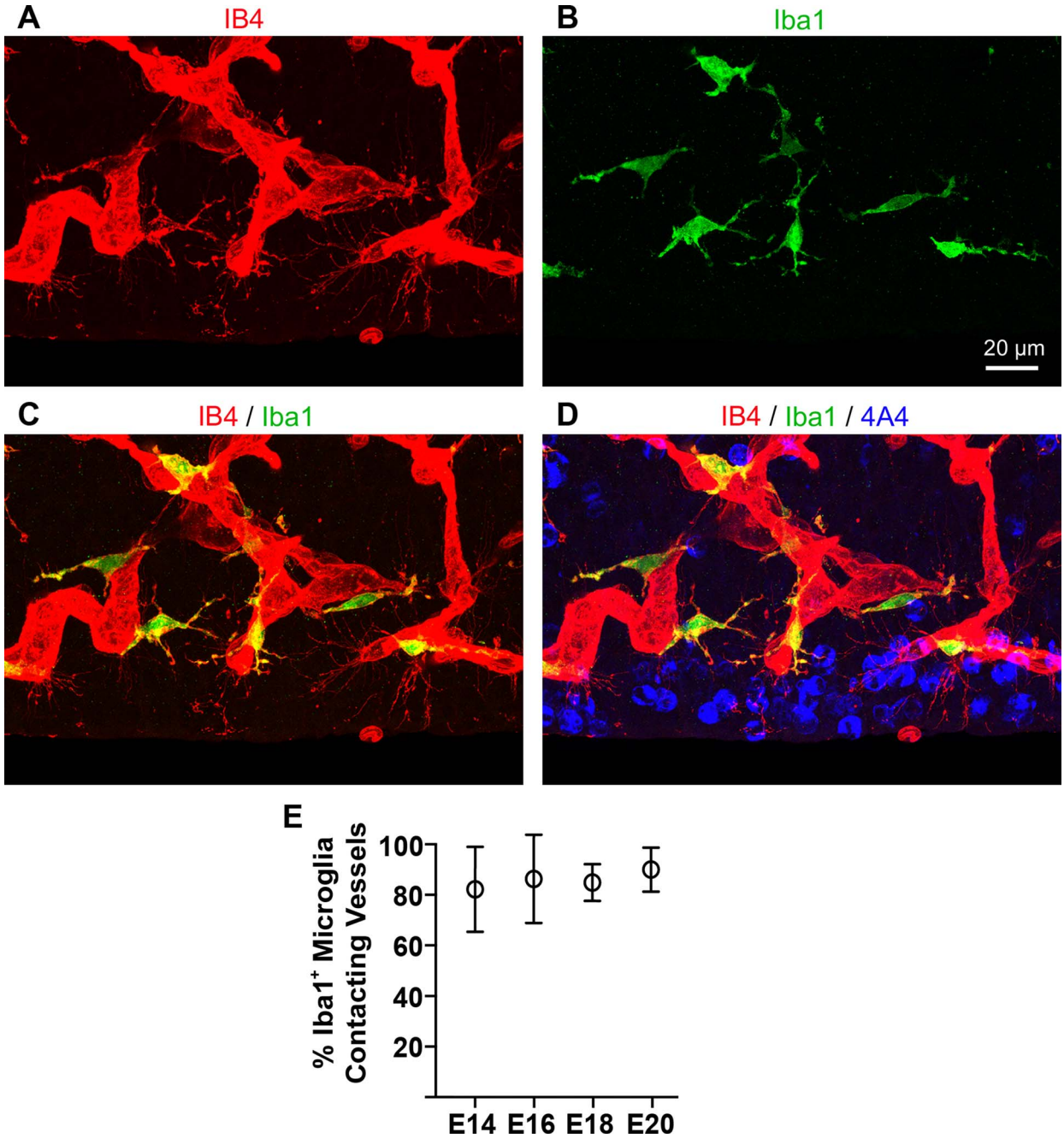

Figure 4. Microglia are closely integrated with isolectin B4 (IB4) labeled blood vessels in the prenatal rat ventricular zone (VZ). (*A*) IB4^{+} vessels (red) in the embryonic day (E)18 rat paraventricular plexus. Note filopodia extending from vessels near the ventricle. (*B*, *C*) Iba1^{+} microglia (green) in the same field of view. Many microglia in the proliferative zones stain positive for both markers (yellow), and are closely affiliated with cortical vessels, especially during early stages of development. (*D*) Merged image showing location of 4A4^{+} mitotic NPCs (blue) dividing at the ventricle in relation to microglia (green) and vessels in the paraventricular plexus (red). (*E*) Between 80—90% of microglia contact blood vessels in the VZ during cortical neurogenesis. One-way ANOVA showed no significant differences between groups. Scale bar in *B* applies to all panels.

rat tissue with IB4 and markers that identify components of cortical vessels including endothelial cells (anti-CD31), pericytes (anti-PDFGR-β, anti-NG2), and smooth muscle cells (anti-α SMA). We found that IB4^{+} vessels in the prenatal rat cortex stained with the endothelial cell marker CD31 (Fig. 7A), confirming the presence of endothelial cells in the prenatal cortical vessels as previously reported (Shen et al. 2004; Engelhardt and Liebner 2014; Bjornsson et al. 2015; da Silva et al. 2019). We also found PDGFR-β^{+} cells (but not NG2^{+} cells) adjacent to and tightly adhered to IB4^{+} vessels (white arrows, Fig. 7B), demonstrating the presence of pericytes along vessel walls as previously described (Engelhardt and Liebner 2014). We did not find evidence for consistent α-SMA^{+} staining on or within vessels in the PVP, suggesting that mature smooth

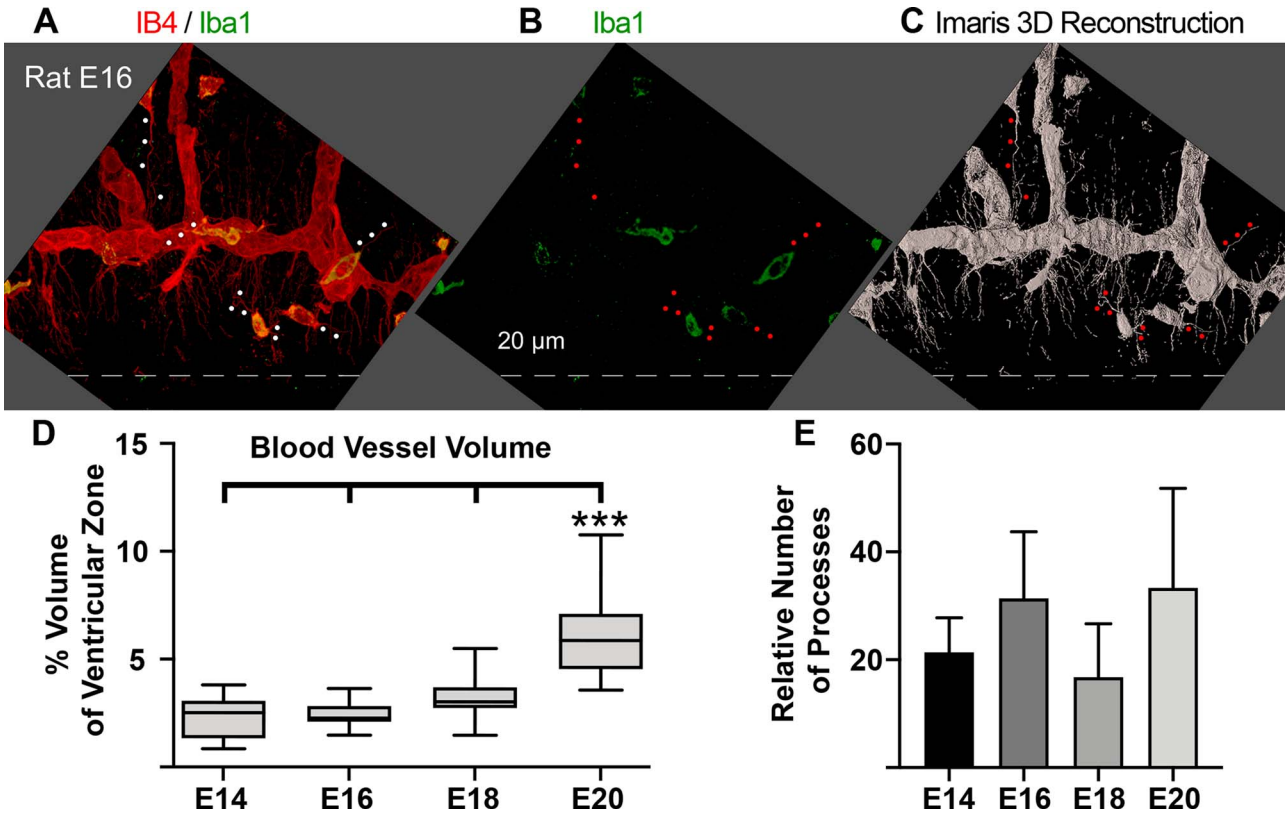

Figure 5. Vessels in the paraventricular plexus extend numerous filopodia directed toward the location of actively dividing NPCs. (*A*, *B*) IB4 labeled vessels (red) in the paraventricular plexus of the embryonic day (E)16 rat. Microglia are stained with Iba1 (green), and express both markers at this stage of development (yellow). Dotted line indicated surface of the lateral ventricle. (*C*) Imaris 3D reconstruction of red IB4^{+} signal shown in panel *A*. Microglial cells and their cellular processes (red dots) were subtracted from volumetric and filopodia analyses. (*D*) The volume of VZ occupied by IB4 vessels increases slowly across development from 2.3% at E14 to 6.2% at E20, and was significantly greater at E20 than at E14, E16, and E18 (One-way ANOVA, Tukey's post hoc test, $^{***}P < 0.0001$). (*E*) Histogram showing that the relative number of filopodia extending from IB4^{+} vessel segments did not differ across development (One-way ANOVA), but remained comparatively constant.

muscle cells were not incorporated in the walls of vessels at this stage of cortical development. Mature astrocytes are not present in the prenatal rat cerebral cortex. Instead, radial glial cells are the astroglial NPCs that reside in the VZ (Misson et al. 1991; Halliday and Cepko 1992; Malatesta et al. 2000; Miyata et al. 2001; Noctor et al. 2001; Tamamaki et al. 2001; Anthony et al. 2004; Noctor et al. 2004) and make multiple contacts with blood vessels (Schmechel and Rakic 1979; Levitt and Rakic 1980; Noctor et al. 2001). Vimentin labels numerous radial glial processes in the VZ of prenatal rats (Pixley and de Vellis 1984; Noctor et al. 2002). Co-staining with IB4 and anti-vimentin antibodies showed that vimentin^{+} processes coursed along vessels in the VZ as previously reported, but that filopodia extending from vessels in the PVP did not express vimentin (Fig. 8). The 3D analysis of the quadruple-stained tissue in confocal Z-stacks indicated that filopodia were extensions of CD31^{+} endothelial cells (Fig. 7*A*). We found expression of CD31 associated with filopodia but not with markers that label pericytes, smooth muscle cells, or astroglial cells. We noted that filopodia also extended from growing tip cells as noted previously (Marin-Padilla 1985; Javaherian and Kriegstein 2009), but the vast majority of filopodia extended from the walls of vessel segments in the PVP aligned parallel to the ventricle (see Fig. 5). Thus, the filopodia do not simply represent growth of the vascular system, but an apparent interaction between vessels and cellular components in cortical proliferative zones.

Blood Vessels Occupy a Consistent Volume near the Ventricular Surface

We next measured the volume of the proliferative zone tissue that was occupied by blood vessels by analyzing IB4^{+} vessels in confocal Z-stacks with Imaris software. Iba1^{+} microglial soma and processes were subtracted from the volumetric measurements. At E14, the volume of VZ occupied by IB4^{+} vessels was relatively low, $2.3 \pm 0.9\%$. The proportion of the VZ occupied by blood vessels increased slowly across prenatal development, reaching $6.2 \pm 2.0\%$ by E20 (Figs 5*C* and *D*), reflecting an increase in the number of vessels close to the ventricle. This corresponded with a constant number of filopodia extending from vessel segments near the ventricle. Yet, the dense network of vessels in the PVP adjacent to mitotic NPCs remained constant throughout cortical neurogenesis.

Blood Vessels, NPCs, and Microglia are Highly Interconnected

Throughout the period of cortical neurogenesis blood vessels and their filopodia, periventricular microglia, and NPCs were located in the same compartment between the PVP and the lateral ventricle (Fig. 9), and made multiple contacts with one another. We have previously shown that microglia make numerous contacts on NPCs, with over 40% of periventricular microglia

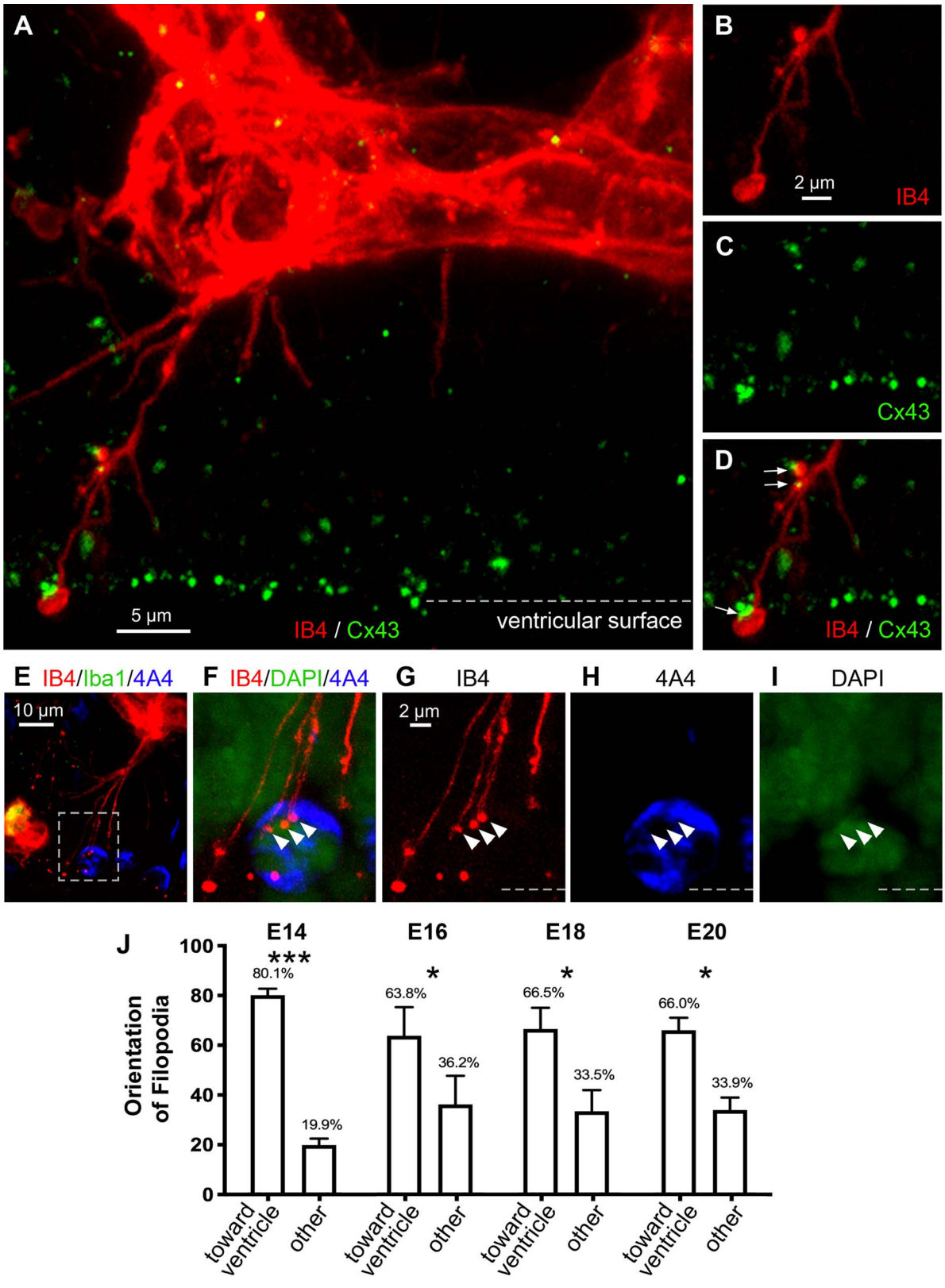

Figure 6. The majority of filopodia processes extending from IB4^{+} vessels were oriented toward the ventricle across development, and were marked by varicosities and terminal enlargements. (*A*) Filopodia extending from an IB4^{+} vessel (red) in the paraventricular plexus of an E16 rat reaches the surface of the ventricle. (*B*) IB4^{+} filopodia (red) are often marked by varicosities and 1—2 µm wide terminal enlargements at the ventricle. (*C*, *D*) Co-staining for IB4 (red) and the gap junction connexin 43 (green, Cx43) shows that Cx43 expression co-localizes with the enlargements on vascular filopodia (white arrows). (*E*) IB4^{+} vascular filopodia extend from a cortical vessel (red) and contact mitotic NPCs (blue) at the ventricular surface. Microglia (green) are often closely affiliated with vasculature and appear yellow. (*F-I*) Higher power images from inset in *E*, show projection images from a confocal Z-stack. (*G*) A vascular filopodia (red) trifurcated, each of the three processes terminating *(legend continued on next page)*

simultaneously contacting three or more mitotic NPCs (Barger et al. 2019; Noctor et al. 2019). In the current analysis, we found that 80—90% of periventricular microglia contacted blood vessels in the PVP between E14 and E20 (Fig. 4E). Statistical analysis showed that the proportion of microglia associated with vessels in the PVP remained constant and did not differ across development. Each microscopic field of view included dozens of $4A4^+$ mitotic NPCs with visible pial processes in direct contact with blood vessels in the PVP. The number of NPC processes that contacted vessels was significantly higher at the start of neurogenesis (E14) compared to the end of cortical neurogenesis at E20 (Fig. 10A). We also observed filopodia extending from vessels in the PVP that made apparent contact with $4A4^+$ mitotic precursor cells at the surface of the ventricle. At E14, $39.6 \pm 12.9\%$ of blood vessel filopodia visibly contacted mitotic NPCs. At E16, $12.0 \pm 10.1\%$ of filopodia contacted mitotic NPCs; at E18, $24.7 \pm 18.6\%$ of blood vessel filopodia visibly contacted mitotic NPCs; and at E20, the proportion of filopodia contacting mitotic NPCs fell to $2.4 \pm 4.0\%$ (Fig. 10B). Cycling NPCs stain positive for the 4A4 antibody for approximately only 2 hours of the 12—20 hour NPC cell cycle (Takahashi et al. 1995; Noctor et al. 2002; Weissman et al. 2003; Noctor et al. 2004). Thus, this analysis considered only the subset of actively dividing NPCs and likely represents a fraction of contacts between vascular filopodia and cycling NPCs in the VZ.

Discussion

Defining the cellular and structural composition of the cortical proliferative zones is central for understanding factors that regulate the function of the precursor cells that produce cortical neurons and glial cells. We previously showed that microglial cells phagocytose NPCs in the prenatal cortex (Cunningham et al. 2013), and make extensive contacts with the soma and processes of NPCs (Barger et al. 2019; Noctor et al. 2019). Here we provide new data showing that the developing vasculature is a critical component in the cortical proliferative zones and contributes to the complex environment in which NPCs and microglia function. Overall, we show an interplay between NPCs, microglia, and vasculature in the developing cortex.

We show that the PVP forms at the onset of cortical neurogenesis adjacent to the actively dividing NPCs that line the ventricle; that this dense vascular network remains in place throughout cortical neurogenesis; that numerous filopodia extend from the PVP—especially toward NPCs undergoing division at the edge of the ventricle; and that expression of the gap junction protein Cx43 is associated with filopodia. We also show a high degree of apparent interconnectivity between blood vessels, dividing precursor cells, and periventricular microglia in the proliferative compartment that lines the lateral ventricles of the prenatal rat cerebrum. Previous work has shown that endothelial cells obtained from the embryonic cortex promote NPC self-renewing divisions in culture (Shen et al. 2004), and that there is a positive correlation between the location of NPCs and blood vessels (Javaherian and Kriegstein 2009; Stubbs et al. 2009). We show that cortical vasculature is highly integrated in the cortical proliferative zones, suggesting that cortical vasculature contributes to the regulation of NPC function through direct contact via filopodial processes. Together, these data are consistent with the concept that the function of NPCs results from signaling and feedback obtained from a variety of sources including the developing vasculature and microglia. Paraphrasing earlier work, the production of neurons and glial cells is inseparable from the development of fundamental components such as the vasculature (Marin-Padilla 1995; Bjornsson et al. 2015).

The Paraventricular Plexus Forms at the Onset of Cortical Neurogenesis

Development of cortical vasculature is first marked by the appearance of a dense vascular plexus in the pial meninges called the perineural vascular plexus or pial capillary plexus (Marin-Padilla 1985; Marin-Padilla and Knopman 2011; Bjornsson et al. 2015; Segarra et al. 2019). Endothelial cells in this pial vascular plexus penetrate the underlying cortical tissue and descend toward the ventricle (Marin-Padilla 1985; see Fig. 2). Soon after the PVP is established as a collection of short vessels in the VZ that course parallel to the ventricle, and that remain in place throughout cortical neurogenesis (Figs 2 and 9). The PVP has been identified as the 'Subventricular Plexus' in previous studies, but we use the term 'paraventricular plexus' since the PVP is located exclusively in the VZ from the onset of neurogenesis at E12 through E16. The SVZ appears as a distinct structure in the rat neocortex after E16 (Bayer and Altman 1991), but vessels in the PVP remain in the VZ throughout neurogenesis. As development proceeds the PVP grows thicker and becomes closely linked with similar vessels that form in the SVZ. A dense bed of anastomotic loops that first appear in the PVP grows thicker in the radial dimension as the SVZ develops, and eventually appears as a continuous plexus extending from the ventricle through the SVZ in the E19/E20 rats (Figs 2E and 3). The growth of the PVP into the SVZ keeps this vascular structure closely affiliated with mitotic NPCs as the bulk of mitoses shifts from the ventricular surface at E12 to the SVZ by E20 in the rat (Martinez-Cerdeño et al. 2012).

Vessels in the PVP Extend Numerous Filopodia that Contact NPCs

Earlier work has shown that endothelial cells extend leading processes and a tip filopodium as vessels grow in the developing cortex (Marin-Padilla 1985), not unlike migrating neurons that extend leading processes as they navigate through cortical layers (McConnell 1985; O'Rourke et al. 1992; Schaar et al. 2004). In addition to tip filopodia, we found that numerous filopodia also extended from the walls of vessels in the PVP (see Fig. 5). Quadruple immunostaining for markers of cell types that comprise cortical vessels, combined with confocal microscopy provided evidence consistent with filopodia emanating from endothelial cells (Figs 7 and 8). The filopodia extended in all directions from the vessels in the PVP, but at least 65% were

Figure 6 continued: with a 1 µm wide bouton-like enlargement (white arrowheads). (*H*, *I*) Z-stack analysis showed that these filopodia enlargements terminated within the $4A4^+$ immunosignal (blue), adjacent to the DAPI-labeled nuclear DNA (green) of this mitotic NPC. Dotted line represents surface of the ventricle. (*J*) Histogram showing that at E14 80% filopodia processes were oriented to the ventricle, and for the remainder of development approximately 65% of filopodia were oriented toward the ventricle. At each age significantly more processes were oriented to the ventricle versus all other directions (One-way ANOVA, Tukey's post hoc test, $^*P < 0.01$, $^{***}P < 0.0001$).

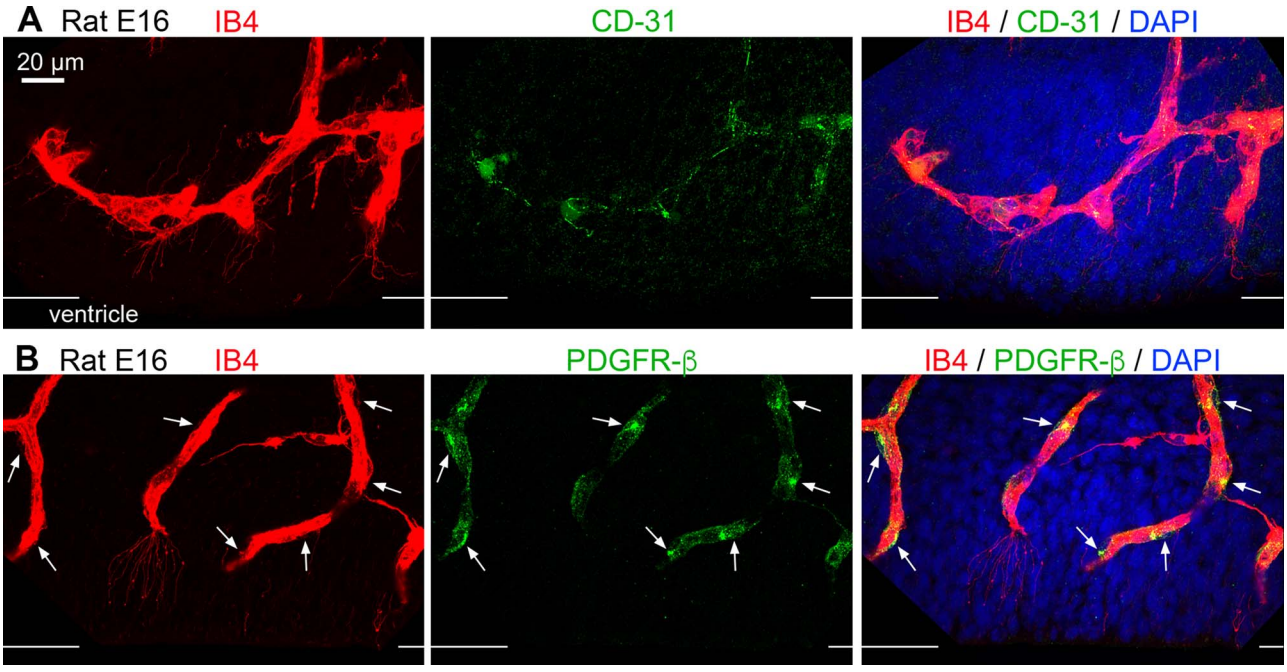

Figure 7. Cortical vessels in the paraventricular plexus are composed of endothelial cells and pericytes. (*A*) IB4$^+$ vessels (red) in the embryonic day (E)16 rat VZ consist of CD-31$^+$ endothelial cells (green). (*B*) PDGFR-β^+ pericytes (green) localize along vessels in the E16 rat paraventricular plexus. Pericytes soma (green) are visible on the perimeter of the vessels (white arrows). Vessels in the paraventricular plexus do not stain positive with antibodies against vascular smooth muscle cell actin (not shown). Thin filopodia extending from the E16 vessels are visible. The surface of the ventricle is marked by white lines of edge of each image. Blue, DAPI.

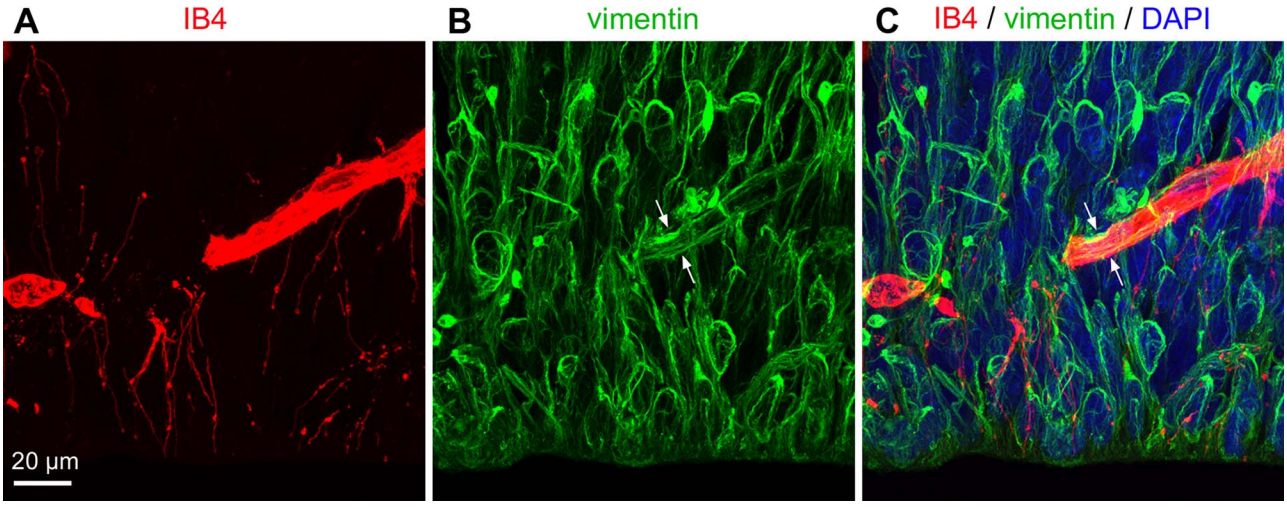

Figure 8. Filopodia are distinct from NPC processes and do not express vimentin. (*A-C*) The filopodial processes from an E18 rat that extend from IB4$^+$ vessels (red) are closely affiliated with radial glial processes, but are distinct from these processes and do not express vimentin (green). Vimentin$^+$ processes coursed around and along the IB4$^+$ vessels in the VZ (white arrows). DAPI (blue). Scale bar in A applies to all panels.

oriented toward the ventricle. Of ventricular-directed processes, 10–40% made direct contact with NPCs dividing at the ventricle (Figs 6*E–I* and 10*B*).

The filopodia extending from vessels in the PVP exhibited different morphological profiles. Some filopodia that contacted NPCs had a uniform diameter from origin to terminus, while other filopodia had varying diameters with varicosities and terminal swellings up to 2 μm in diameter. The terminal swellings were often located at the ventricular surface, and we noted that expression of the connexin Cx43 was adjacent to and overlapped with the terminal swellings (Fig. 6). Cx43 is expressed by astrocytes (Verkhratsky and Nedergaard 2018), and by astroglial cells such as radial glial NPCs (Bittman et al. 1997; Nadarajah et al. 1997; Bittman and LoTurco 1999). Cx43 forms homomeric and heteromeric channels with adjacent cells that express Cx43 or other connexins, and also forms hemichannels that serve as gated pores (Weissman et al. 2004; Verkhratsky and Nedergaard 2018). Gap junction channels serve to electrically couple adjacent radial glial NPCs in the VZ (LoTurco and Kriegstein 1991; Bittman et al. 1997), and hemichannels have been shown to

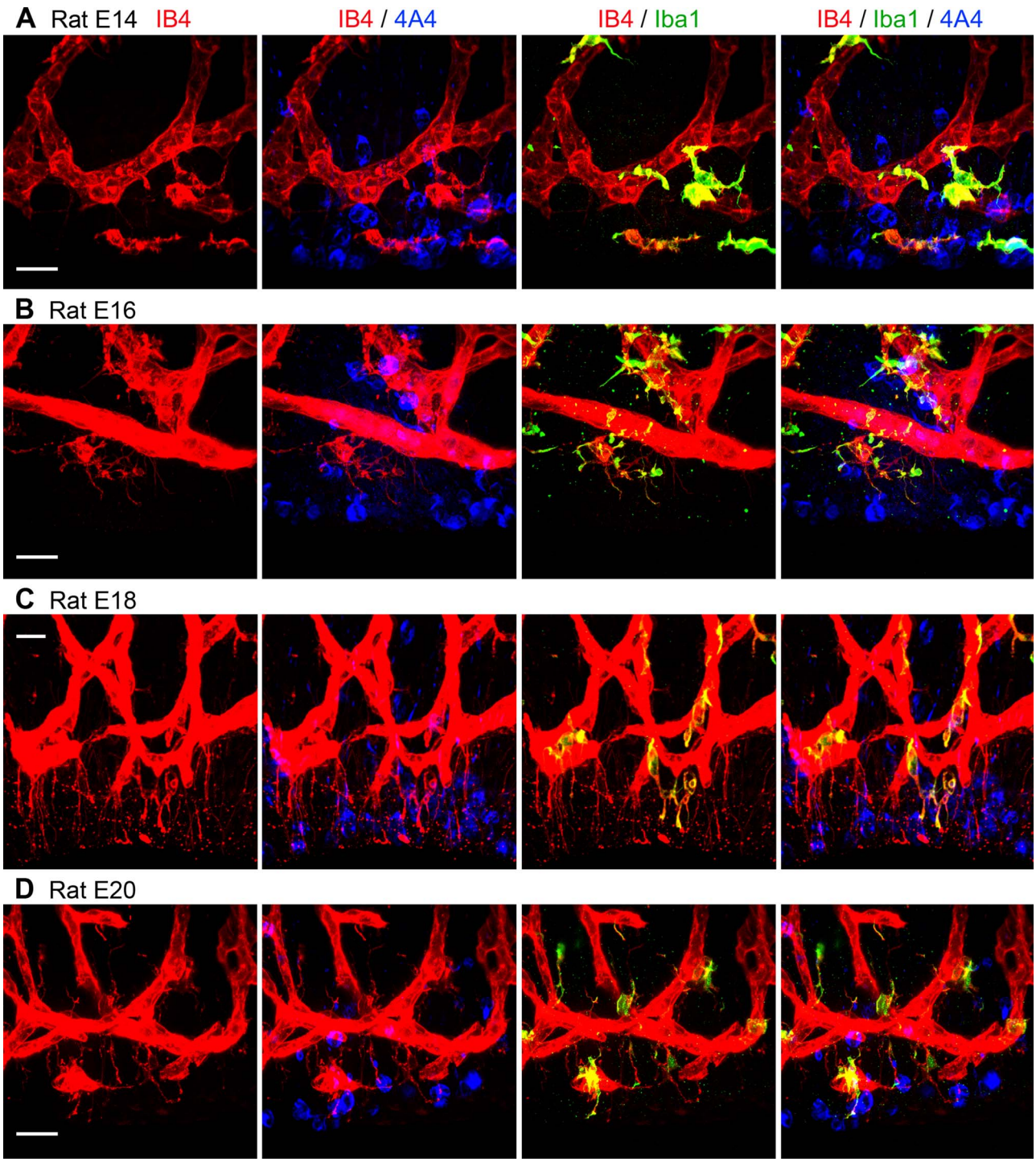

Figure 9. IB4^{+} vessels, microglial cells, and mitotic NPCs are tightly interconnected in the embryonic rat proliferative zones between the PVP and the ventricle. (*A-D*) Vessels in the paraventricular plexus (red), microglia (green), and actively dividing NPCs (blue) are in contact with each other throughout the period of cortical neurogenesis. Scale bars = 20 µm.

regulate NPC proliferation (Weissman et al. 2004). Cx43 is also expressed by migrating neurons (Nadarajah et al. 1997; Cina et al. 2007), serving to regulate neuronal migration in the developing brain (Elias et al. 2007; Cina et al. 2009; Elias et al. 2010). Published reports also support expression of Cx43 by endothelial cells (Okamoto et al. 2019), specifically in rat brain (De Bock et al. 2011; Belousov et al. 2017), in fetal human telencephalon (Errede et al. 2002), and by radial glial NPCs at their interface with endothelial cells in the human brain (Errede et al. 2014). Cx43 regulates essential endothelial cell functions including angiogenesis (Chen et al. 2015), migration (Kameritsch et al. 2019; Okamoto et al. 2019), and formation of the blood–brain barrier

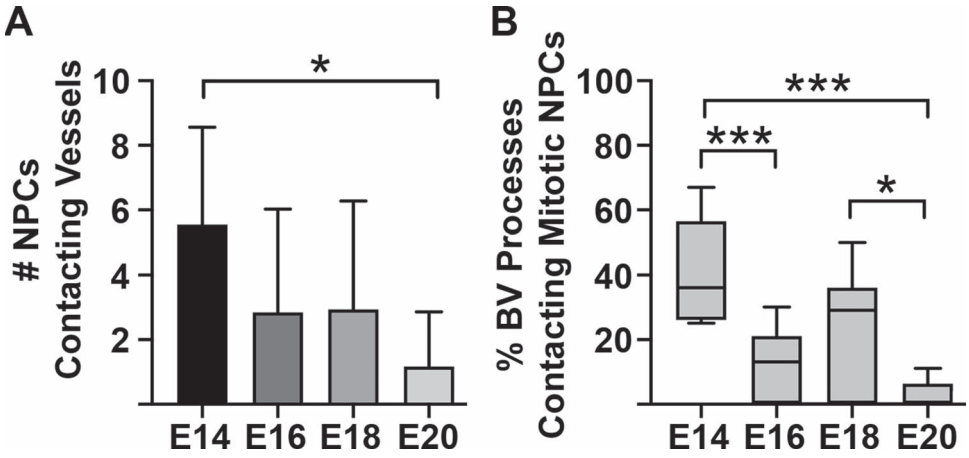

Figure 10. Graphs showing interconnectivity between blood vessels and mitotic NPCs in the embryonic rat VZ. (*A*) The relative number of soma and processes of actively dividing NPCs that contact blood vessels is significantly higher at the onset compared to the end of cortical neurogenesis (Kruskal–Wallis ANOVA, Dunn's post hoc test, $^{*}P < 0.01$). (*B*) Histogram showing the proportion of blood vessel filopodia that contact mitotic NPCs during neurogenesis. Nearly 40% of filopodia contact mitotic NPCs undergoing cytokinesis at the ventricle in the E14 brain. Mitotic NPCs stain positive with 4A4 only during M-phase, approximately 2 hours during the entire cell cycle. Statistical analysis showed significant differences between E14 versus E16 & E20 (One-way ANOVA, Tukey's post hoc test, $^{***}P < 0.0001$), and E18 versus E20 (One-way ANOVA, Tukey's post hoc test, $^{*}P < 0.01$). This analysis did not quantify contacts between filopodia and the interphase NPCs that are not labeled with 4A4.

junction complex (Johnson et al. 2018). Our data showing Cx43 expression adjacent to and overlapping with vascular filopodia at the edge of the ventricle are consistent with previous findings of Cx43 expression by endothelial cells and suggest that gap junctions or hemichannels may serve as a conduit for communication between endothelial cells and NPCs. Further supporting this interpretation, we also noted terminal swellings of filopodia that seemingly penetrated the soma of $4A4^{+}$ dividing cells (Figs 6*E–I*). These findings provide evidence that mitotic NPCs may have a complex outer surface with depressions, grooves, or channels through which cellular processes and filopodia course. In addition, the data provide more evidence for direct intercellular communication between endothelial cells and NPCs. Together these data support the concept that vessels in the PVP are more than conduits for blood supply, but rather interactive structures that extend numerous filopodia to contact NPCs and other cell types. Previous work has shown that endothelial cells release soluble factors that influence NPC behavior including self-renewal (Shen et al. 2004). Our results indicate this signaling could occur at close range. Additional explanations for contacts between vasculature and NPCs include feed-forward signaling in which endothelial cells induce specific NPC behavior or influence daughter cell fate decisions, as well as feedback signaling from NPCs to regulate key functions identified for endothelial cells, such as vasculogenesis, stabilization of cortical vessels (Errede et al. 2014), or regulation of blood flow in proliferative regions with high metabolic demands. The data we present here suggest that endothelial cells communicate via gap junctions, hemichannels, or release of secretable factors with neighboring cells including NPCs. We cannot rule out the possibility that Cx43 protein was expressed by neighboring cells at the edge of the ventricle, including NPCs undergoing cytokinesis or in other phases of the cell cycle, newborn neurons, or microglia. Consistent with this interpretation, whole-cell recordings and intracellular dye filling of radial glial cells using low molecular weight dyes that can pass through gap junction channels have not reported labeling of vascular structures (LoTurco and Kriegstein 1991; Bittman et al. 1997). But as discussed above, additional cell types are present at the surface of the ventricle including microglia (Cunningham et al. 2013; Barger et al. 2019), which also express Cx43 (Gajardo-Gomez et al. 2016).

Neuro-Immune-Vascular Triad

A key aspect of this work highlights the affiliations between vasculature, NPCs, and microglia in the developing cerebral cortex. Previous studies have reported associations between pairs of these elements. For example, radial glial cell contact with blood vessels was noted in the 19th century (Golgi 1886), has been well characterized (Schmechel and Rakic 1979; Misson et al. 1988; Voigt 1989), and noted specifically for neurogenic radial glial cells (Noctor et al. 2001). These findings matched work in the adult SVZ that showed an affiliation between neurogenic astrocytes and cortical vessels (Alvarez-Buylla and Garcia-Verdugo 2002). An affiliation between $Tbr2^{+}$ intermediate NPCs and cortical vessels has also been reported (Javaherian and Kriegstein 2009; Stubbs et al. 2009). The affinity of microglia for blood vessels (Rezaie and Male 1999), and NPCs (Cunningham et al. 2013) has also been shown in previous work. Furthermore, the concept of neuroglial-vascular units as functional partners in both the mature and developing brain is becoming widely appreciated (Segarra et al. 2019). Our data previous publications by showing the complex morphology of blood vessel filopodia in the embryonic rat VZ (Figs 4, 5, 6, and 9), that microglia are essential components in neuro-vascular units, and that blood vessels, microglial cells, and NPCs are tightly interwoven in the confined space between the lateral ventricle and the PVP. These data indicate that blood vessels, microglial cells, and NPCs may function as a neuro-immune-vascular unit in the prenatal cerebral cortex.

Health Implications

Pathology associated with infectious diseases such as ZIKV and SARS-COV-2 show that endothelial cells and microglia are susceptible to infection, including in the fetal brain

(Lum et al. 2017; Papa et al. 2017; Ackermann et al. 2020; Labo et al. 2020). Endothelial cells may thus serve as a route for spreading infection widely throughout the body and also an entry point for infectious diseases into the brain. ZIKV has been shown to infect NPCs (Dang et al. 2016; Garcez et al. 2016; Tang et al. 2016), and has also been associated with enlarged cerebral vessels exhibiting abnormal morphology in fetal rhesus monkey and ferret (Hutchinson et al. 2019; Tarantal et al. 2020), and with impaired development of cerebral vasculature in mouse models (Shao et al. 2016; Garcez et al. 2018). Given the complex interconnectivity we show here between vessels, NPCs, and microglia in the normally developing cerebrum (Fig. 9), endothelial cells that become functionally impaired through infection may further compromise nervous system development. Indeed, we have found that Zika administration to fetal rhesus monkeys produced abnormalities in microglial cell and $Tbr2^{+}$ cell distribution, blood vessel morphology, and is correlated with thinner cortical gray matter (Tarantal et al. 2020). Other conditions including schizophrenia, hydrocephaly, and children born of pre-eclamptic pregnancies have also been correlated with vascular abnormalities (Webster et al. 2001; Lara et al. 2018; Fehnel et al. 2019). Cortical gray matter reduction in schizophrenia has been associated with both neuroinflammation (Zhang et al. 2016) and altered levels of the vascular growth factor VEGF (Pillai et al. 2016). Inflammation and vascular abnormalities that have been reported in some neurodevelopmental disorders may occur in the mature brain as downstream effects of disease progress or even medication. However, microglial activation and release of pro-inflammatory cytokines have been shown to decrease Cx43 expression in astrocytes in animal models (Retamal et al. 2007; Watanabe et al. 2016). Therefore, inflammation in the developing brain may impair intercellular signaling between NPCs, microglia, and endothelial cells, potentially altering the typical trajectory of neurodevelopment, and increasing the risk for onset of neurodevelopmental disorders. The intersection of microglial cells, vasculature, and NPCs in the developing brain amplifies the importance of understanding how the neuro-immune-vascular unit contributes to brain development, especially given the susceptibility of endothelial cells and microglia to extrinsic pathogens.

Funding

The NIH (grants MH101188 and NS109379 to S.C.N.); the UC Davis MIND Institute (IDDRC, U54 HD079125); the UC Davis Department of Psychiatry.

Notes

Conflict of interest: The authors have no financial interests that would represent a conflict of interest.

References

Ackermann M, Verleden SE, Kuehnel M, Haverich A, Welte T, Laenger F, Vanstapel A, Welein C, Stark H, Tzankov A *et al.* 2020. Pulmonary vascular Endothelialitis, thrombosis, and angiogenesis in Covid-19. *N Engl J Med*. 383:120–128.

Alvarez-Buylla A, Garcia-Verdugo JM. 2002. Neurogenesis in adult subventricular zone. *J Neurosci*. 22:629–634.

Andjelkovic AV, Nikolic B, Pachter JS, Zecevic N. 1998. Macrophages/microglial cells in human central nervous system during development: an immunohistochemical study. *Brain Res*. 814:13–25.

Angelov DN, Vasilev VA. 1989. Morphogenesis of rat cranial meninges. A light- and electron-microscopic study. *Cell Tissue Res*. 257:207–216.

Anthony TE, Klein C, Fishell G, Heintz N. 2004. Radial glia serve as neuronal progenitors in all regions of the central nervous system. *Neuron*. 41:881–890.

Barger N, Keiter J, Kreutz A, Krishnamurthy A, Weidenthaler C, Martinez-Cerdeno V, Tarantal AF, Noctor SC. 2019. Microglia: an intrinsic component of the proliferative zones in the Fetal rhesus monkey (Macaca mulatta) cerebral cortex. *Cereb Cortex*. 29:2782–2796.

Bayer SA, Altman J. 1991. *Neocortical Development*. New York: Raven Press.

Belousov AB, Fontes JD, Freitas-Andrade M, Naus CC. 2017. Gap junctions and hemichannels: communicating cell death in neurodevelopment and disease. *BMC Cell Biol*. 18:1–11.

Bentivoglio M, Mazzarello P. 1999. The history of radial glia. *Brain Res Bull*. 49:305–315.

Bittman K, Owens DF, Kriegstein AR, LoTurco JJ. 1997. Cell coupling and uncoupling in the ventricular zone of developing neocortex. *J Neurosci*. 17:7037–7044.

Bittman KS, LoTurco JJ. 1999. Differential regulation of connexin 26 and 43 in murine neocortical precursors. *Cereb Cortex*. 9:188–195.

Bjornsson CS, Apostolopoulou M, Tian Y, Temple S. 2015. It takes a village: constructing the neurogenic niche. *Dev Cell*. 32:435–446.

Chen CH, Mayo JN, Gourdie RG, Johnstone SR, Isakson BE, Bearden SE. 2015. The connexin 43/ZO-1 complex regulates cerebral endothelial F-actin architecture and migration. *Am J Physiol Cell Physiol*. 309:600–607.

Cina C, Bechberger JF, Ozog MA, Naus CC. 2007. Expression of connexins in embryonic mouse neocortical development. *J Comp Neurol*. 504:298–313.

Cina C, Maass K, Theis M, Willecke K, Bechberger JF, Naus CC. 2009. Involvement of the cytoplasmic C-terminal domain of connexin43 in neuronal migration. *J Neurosci*. 29:2009–2021.

Cunningham CL, Martinez-Cerdeno V, Noctor SC. 2013. Microglia regulate the number of neural precursor cells in the developing cerebral cortex. *J Neurosci*. 33:4216–4233.

da Silva SM, Campos GD, Gomes FCA, Stipursky J. 2019. Radial glia-endothelial Cells' bidirectional interactions control vascular maturation and astrocyte differentiation: impact for blood-brain barrier formation. *Curr Neurovasc Res*. 16:291–300.

Dang J, Tiwari SK, Lichinchi G, Qin Y, Patil VS, Eroshkin AM, Rana TM. 2016. Zika virus depletes neural progenitors in human cerebral organoids through activation of the innate immune receptor TLR3. *Cell Stem Cell*. 19:258–265.

De Bock M, Culot M, Wang N, Bol M, Decrock E, De Vuyst E, da Costa A, Dauwe I, Vinken M, Simon AM *et al.* 2011. Connexin channels provide a target to manipulate brain endothelial calcium dynamics and blood–brain barrier permeability. *J Cerebral Blood Flow and Metabolism : Official J Int Society of Cerebral Blood Flow and Metabolism*. 31:1942–1957.

Elias LA, Turmaine M, Parnavelas JG, Kriegstein AR. 2010. Connexin 43 mediates the tangential to radial migratory switch in ventrally derived cortical interneurons. *J Neurosci*. 30:7072–7077.

Elias LA, Wang DD, Kriegstein AR. 2007. Gap junction adhesion is necessary for radial migration in the neocortex. *Nature*. 448:901–907.

Engelhardt B, Liebner S. 2014. Novel insights into the development and maintenance of the blood-brain barrier. *Cell Tissue Res*. 355:687–699.

Errede M, Benagiano V, Girolamo F, Flace P, Bertossi M, Roncali L, Virgintino D. 2002. Differential expression of connexin43 in foetal, adult andtumour-associated human brain endothelial cells. *Histochem J*. 34:265–271.

Errede M, Girolamo F, Rizzi M, Bertossi M, Roncali L, Virgintino D. 2014. The contribution of CXCL12-expressing radial glia cells to neuro-vascular patterning during human cerebral cortex development. *Front Neurosci*. 8:1–11.

Fehnel KP, Klein J, Warf BC, Smith ER, Orbach DB. 2019. Reversible intracranial hypertension following treatment of an extracranial vascular malformation: case report. *J Neurosurg Pediatr*. 23:369–373.

Gajardo-Gomez R, Labra VC, Orellan JA. 2016. Connexins and pannexins: new insights into microglial functions and dysfunctions. *Frontiers in Molecular Neuroscience*. 9:1–19.

Garcez PP, Loiola EC, da Costa RM, Higa LM, Trindade P, Delvecchio R, Nascimento JM, Brindeiro R, Tanuri A, Rehen SK. 2016. Zika virus impairs growth in human neurospheres and brain organoids. *Science*. 352:816–818.

Garcez PP, Stolp HB, Sravanam S, Christo RR, Ferreira JCCG, Dias AA, Pezzuto P, Higa LM, Barbeito-Andrés J, Ferreira RO *et al*. 2018. Zika virus impairs development of blood vessels in a mouse model of congenital infection. *Sci Rep*. 8:12774.

Golgi C. 1886. *Sulla fina anatomia degli organi centrali del sistema nervoso*. Milano: Hoepli.

Halliday AL, Cepko CL. 1992. Generation and migration of cells in the developing striatum. *Neuron*. 9:15–26.

Hutchinson EB, Chatterjee M, Reyes L, Djankpa FT, Valiant WG, Dardzinski B, Mattapallil JJ, Pierpaoli C, Juliano SL. 2019. The effect of Zika virus infection in the ferret. *J Comp Neurol*. 527:1706–1719.

Iadecola C. 2017. The neurovascular unit coming of age: a journey through neurovascular coupling in health and disease. *Neuron*. 96:17–42.

Javaherian A, Kriegstein A. 2009. A stem cell niche for intermediate progenitor cells of the embryonic cortex. *Cereb Cortex*. 19(Suppl 1):i70–i77.

Johnson AM, Roach JP, Hu A, Stamotovic SM, Zochowski MR, Keep RF, Andjelkovic AV. 2018. Connexin 43 gap junctions contribute to brain endothelial barrier hyperpermeability in familial cerebral cavernous malformations type III by modulating tight junction structure. *FASEB J*. 32:2615–2629.

Kameritsch P, Kiemer F, Mannell H, Beck H, Pohl U, Pogoda K. 2019. PKA negatively modulates the migration enhancing effect of Connexin 43. *Biochem Biophys Acta Mol Cell Res*. 1865:828–838.

Kisler K, Nelson AR, Montagne A, Zlokovic BV. 2017. Cerebral blood flow regulation and neurovascular dysfunction in Alzheimer disease. *Nat Rev Neurosci*. 18:419–434.

Labo N, Ohnuki H, Tosato G. 2020. Vasculopathy and coagulopathy associated with SARS-CoV-2 infection. *Cell*. 9:1–30.

Lara E, Acurio J, Leon J, Penny J, Torres-Vergara P, Escudero C. 2018. Are the cognitive alterations present in children born from Preeclamptic pregnancies the result of impaired angiogenesis? Focus on the potential role of the VEGF family. *Front Physiol*. 9:1–10.

Levitt P, Rakic P. 1980. Immunoperoxidase localization of glial fibrillary acidic protein in radial glial cells and astrocytes of the developing rhesus monkey brain. *J Comp Neurol*. 193:815–840.

LoTurco JJ, Kriegstein AR. 1991. Clusters of coupled neuroblasts in embryonic neocortex. *Science*. 252:563–566.

Lum F-H, Low DKS, Fan Y, Tan JJL, Lee B, Chan JKY, Renia L, Ginhoux F, Ng LFP. 2017. Zika virus infects human Fetal brain microglia and induces inflammation. *Clin Infect Dis*. 64:914–920.

Malatesta P, Hartfuss E, Gotz M. 2000. Isolation of radial glial cells by fluorescent-activated cell sorting reveals a neuronal lineage. *Development*. 127:5253–5263.

Marin-Padilla M. 1985. Early vascularization of the embryonic cerebral cortex: Golgi and electron microscopic studies. *J Comp Neurol*. 241:237–249.

Marin-Padilla M. 1995. Prenatal development of fibrous (white matter), protoplasmic (gray matter), and layer I astrocytes in the human cerebral cortex: a Golgi study. *J Comp Neurol*. 357:554–572.

Marin-Padilla M, Knopman DS. 2011. Developmental aspects of the intracerebral microvasculature and perivascular spaces: insights into brain response to late-life diseases. *J Neuropathol Exp Neurol*. 70:1060–1069.

Martinez-Cerdeño V, Cunningham CL, Camacho J, Antczak JL, Prakash AN, Cziep ME, Walker AI, Noctor SC. 2012. Comparative analysis of the subventricular zone in rat, ferret and macaque: evidence for an outer subventricular zone in rodents. *PLoS One*. 7:e30178.

Mastorakos P, McGavern D. 2019. The anatomy and immunology of vasculature in the central nervous system. *Science Immunology*. 4:eaav0492.

McConnell SK. 1985. Migration and differentiation of cerebral cortical neurons after transplantation into the brains of ferrets. *Science*. 229:1268–1271.

Misson JP, Edwards MA, Yamamoto M, Caviness VS Jr. 1988. Identification of radial glial cells within the developing murine central nervous system: studies based upon a new immunohistochemical marker. *Brain Res Dev Brain Res*. 44:95–108.

Misson JP, Takahashi T, Caviness VS Jr. 1991. Ontogeny of radial and other astroglial cells in murine cerebral cortex. *Glia*. 4:138–148.

Miyata T, Kawaguchi A, Okano H, Ogawa M. 2001. Asymmetric inheritance of radial glial fibers by cortical neurons. *Neuron*. 31:727–741.

Nadarajah B, Jones AM, Evans WH, Parnavelas JG. 1997. Differential expression of connexins during neocortical development and neuronal circuit formation. *J Neurosci*. 17:3096–3111.

Noctor SC, Flint AC, Weissman TA, Dammerman RS, Kriegstein AR. 2001. Neurons derived from radial glial cells establish radial units in neocortex. *Nature*. 409:714–720.

Noctor SC, Flint AC, Weissman TA, Wong WS, Clinton BK, Kriegstein AR. 2002. Dividing precursor cells of the embryonic cortical ventricular zone have morphological and molecular characteristics of radial glia. *J Neurosci*. 22:3161–3173.

Noctor SC, Martínez-Cerdeño V, Ivic L, Kriegstein AR. 2004. Cortical neurons arise in symmetric and asymmetric division zones and migrate through specific phases. *Nat Neurosci*. 7:136–144.

Noctor SC, Martinez-Cerdeño V, Kriegstein AR. 2008. Distinct behaviors of neural stem and progenitor cells underlie cortical neurogenesis. *J Comp Neurol*. 508:28–44.

Noctor SC, Penna E, Shepherd H, Chelson C, Barger N, Martinez-Cerdeno V, Tarantal AF. 2019. Periventricular microglial cells interact with dividing precursor cells in the nonhuman primate and rodent prenatal cerebral cortex. *J Comp Neurol*. 527:1598–1609.

O'Rourke NA, Dailey ME, Smith SJ, McConnell SK. 1992. Diverse migratory pathways in the developing cerebral cortex. *Science*. 258:299–302.

Okamoto T, Usuda H, Tanaka T, Wada K, Shimaoka M. 2019. The functional implications of endothelial gap junctions and cellular mechanics in vascular angiogenesis. *Cancer*. 11:237–255.

Paolicelli RC, Bolasco G, Pagani F, Maggi L, Scianni M, Panzanelli P, Giustetto M, Ferreira TA, Guiducci E, Dumas L *et al*. 2011. Synaptic pruning by microglia is necessary for normal brain development. *Science*. 333:1456–1458.

Papa MP, Meuren LM, Coelho SVA, De Oliveira Lucas CG, Mustafa YM, Matassoli FL, Silveira PS, Frost PS, Pezzuto P, Ribeiro MR *et al*. 2017. Zika virus infects, activates, and crosses brain microvascular endothelial cells, without barrier disruption. *Front Microbiol*. 8:1–17.

Pillai A, Howell KR, Ahmed AO, Weinberg D, Allen KM, Bruggemann J, Lenroot R, Liu D, Galletly C, Weickert CS *et al*. 2016. Association of serum VEGF levels with prefrontal cortex volume in schizophrenia. *Mol Psychiatry*. 21:686–692.

Pixley SK, de Vellis J. 1984. Transition between immature radial glia and mature astrocytes studied with a monoclonal antibody to vimentin. *Brain Res*. 317:201–209.

Retamal MA, Froger N, Palacios-Prado N, Ezan P, Saez PJ, Saez JC, Giaume C. 2007. Cx43 hemichannels and gap junction channels in astrocytes are regulated oppositely by proinflammatory cytokines released from activated microglia. *J Neurosci*. 27:13781–13792.

Rezaie P, Male D. 1999. Colonisation of the developing human brain and spinal cord by microglia: a review. *Microsc Res Tech*. 45:359–382.

Schaar BT, Kinoshita K, McConnell SK. 2004. Doublecortin microtubule affinity is regulated by a balance of kinase and phosphatase activity at the leading edge of migrating neurons. *Neuron*. 41:203–213.

Schafer DP, Lehrman EK, Kautzman AG, Koyama R, Mardinly AR, Yamasaki R, Ransohoff RM, Greenberg ME, Barres BA, Stevens B. 2012. Microglia sculpt postnatal neural circuits in an activity and complement-dependent manner. *Neuron*. 74:691–705.

Schmechel DE, Rakic P. 1979. A Golgi study of radial glial cells in developing monkey telencephalon: morphogenesis and transformation into astrocytes. *Anat Embryol*. 156:115–152.

Segarra M, Aburto MR, Hefendehl J, Acker-Palmer A. 2019. Neurovascular interactions in the nervous system. *Annu Rev Cell Dev Biol*. 35:615–635.

Shao Q, Herrlinger S, Yang S-L, Lai F, Moore JM, Brindley MA, Chen J-F. 2016. Zika virus infection disrupts neurovascular development and results in postnatal microcephaly with brain damage. *Development*. 143:4127–4136.

Shen Q, Goderie SK, Jin L, Karanth N, Sun Y, Abramova N, Vincent P, Pumiglia K, Temple S. 2004. Endothelial cells stimulate self-renewal and expand neurogenesis of neural stem cells. *Science*. 304:1338–1340.

Sidman RL, Rakic P. 1973. Neuronal migration, with special reference to developing human brain: a review. *Brain Res*. 62:1–35.

Squarzoni P, Oller G, Hoeffel G, Pont-Lezica L, Rostaing P, Low D, Bessis A, Ginhoux F, Garel S. 2014. Microglia modulate wiring of the embryonic forebrain. *Cell Rep*. 8:1271–1279.

Stubbs D, DeProto J, Nie K, Englund C, Mahmud I, Hevner R, Molnar Z. 2009. Neurovascular congruence during cerebral cortical development. *Cereb Cortex*. 19(Suppl 1): i32–i41.

Takahashi T, Nowakowski RS, Caviness V Jr. 1995. The cell cycle of the pseudostratified ventricular epithelium of the embryonic murine cerebral wall. *J Neurosci*. 15: 6046–6057.

Tamamaki N, Nakamura K, Okamoto K, Kaneko T. 2001. Radial glia is a progenitor of neocortical neurons in the developing cerebral cortex. *Neurosci Res*. 41:51–60.

Tang H, Hammack C, Ogden SC, Wen Z, Qian X, Li Y, Yao B, Shin J, Zhang F, Lee EM *et al*. 2016. Zika virus infects human cortical neural progenitors and attenuates their growth. *Cell Stem Cell*. 18(5):587–590.

Tarantal AF, Hartigan-O'Connor DJ, Penna E, Kreutz A, Martinez ML, Noctor SC. 2020. Fetal rhesus monkey first trimester Zika virus infection impacts cortical development in the second and third trimesters. *Cereb Cortex*. in press.

Ueno M, Fujita Y, Tanaka T, Nakamura Y, Kikuta J, Ishii M, Yamashita T. 2013. Layer V cortical neurons require microglial support for survival during postnatal development. *Nat Neurosci*. 16:543–551.

Verkhratsky A, Nedergaard M. 2018. Physiology of Astroglia. *Physiol Rev*. 98:239–389.

Verney C, Monier A, Fallet-Bianco C, Gressens P. 2010. Early microglial colonization of the human forebrain and possible involvement in periventricular white-matter injury of preterm infants. *J Anat*. 217:436–448.

Voigt T. 1989. Development of glial cells in the cerebral wall of ferrets: direct tracing of their transformation from radial glia into astrocytes. *J Comp Neurol*. 289:74–88.

Watanabe M, Masaki K, Yamasaki R, Kawanokuchi J, Takeuchi H, Matsuishita T, Suzumura A, Kira J-I. 2016. Th1 cells downregulate connexin 43 gap junctions in astrocytes via microglial activation. *Sci Rep*. 6:1–14.

Webster MJ, Knable MB, Johnston-Wilson N, Nagata K, Inagaki M, Yolken RH. 2001. Immunohistochemical localization of phosphorylated GlialFibrillary acidic protein in the prefrontal cortex and Hippocampusfrom patients with schizophrenia, bipolar disorder, and depression. *Brain Behav Immun*. 15:388–400.

Weissman T, Noctor SC, Clinton BK, Honig LS, Kriegstein AR. 2003. Neurogenic radial glial cells in reptile, rodent and human: from mitosis to migration. *Cereb Cortex*. 13:550–559.

Weissman TA, Riquelme PA, Ivic L, Flint AC, Kriegstein AR. 2004. Calcium waves propagate through radial glial cells and modulate proliferation in the developing neocortex. *Neuron*. 43:647–661.

Zhang Y, Catts VS, Sheedy D, McCrossin T, Kril JJ, Weickert CS. 2016. Cortical grey matter volume reduction in people with schizophrenia is associated with neuro-inflammation. *Transl Psychiatry*. 6:e982.